Inorganic Chemistry

ARTICLE

pubs.acs.org/IC

Stack Pattern of the Countercation-Modulating Magnetic Property of Low-Dimensional $[Pt(mnt)_2]^-$ Monoanion Spin Systems

Wen-Bo Pei,[†] Jian-Sheng Wu,[†] Zheng-Fang Tian,[†] Xiao-Ming Ren,*[,†,‡] and You Song[‡]

[†]State Key Laboratory of Materials-Oriented Chemical Engineering and College of Science, Nanjing University of Technology, Nanjing 210009, P.R. China

[‡]State Key Lab & Coordination Chemistry Institute, Nanjing University, Nanjing 210093, P.R. China

Supporting Information

ABSTRACT: Three [1-*N*-(4′-R-benzyl)-4-aminopyridinium][$Pt(mnt)_2$] compounds were structurally and magnetically characterized, where the substituent was attached to the para-position of the phenyl ring (R = CN (**1**), Cl (**2**), and H (**3**); mnt^{2-} = maleonitriledithiolate). **1** and **2** crystallized in the monoclinic space group $P2(1)/c$, with the cations and anions forming segregated columnar stacks. Their structural differences involved two aspects: (1) both anion and cation stacks were regular in **1** and irregular in **2**; (2) the neighboring cations were arranged in the boat-type pattern in **1**, whereas these cations were in the chair-type pattern in **2** within the cation stack. **3** belonged to the triclinic space group $P\bar{1}$, where the anions were assembled into the stack with a tetrameric $[Pt(mnt)_2]^-$ subunit, but the cations did not form the columnar stack. Magnetic measurements disclosed that a spin-Peierls-type transition occurred around 240 K for **1**, whereas a long-range, antiferromagnetic ordering took place at about 5.8 K, and a metamagnetic phenomenon was observed with $H_C \approx 1000$ Oe for **2**; **3** showed very strong antiferromagnetic interactions with diamagnetism in the temperature range 5−300 K. Combined with our previous studies, the correlation between the stacking pattern of benzylpyridinium derivatives in a cation stack and the spin-Peierls-type transition is discussed for the series of quasi-1-D $[M(mnt)_2]^-$ (M = Ni, Pd and Pt) compounds.

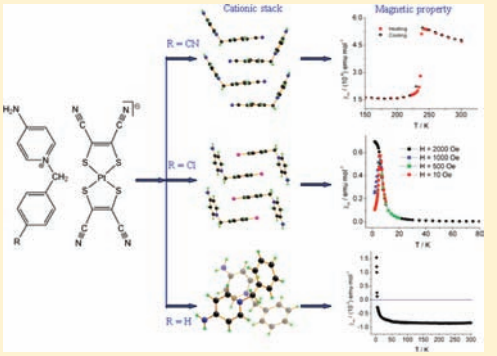

INTRODUCTION

One-dimensional (1-D) molecular solids have recently attracted widespread attention because of their novel physical properties, such as the Peierls transition,[1] spin-Peierls transition,[2] charge-density-wave (CDW)/spin-density-wave (SDW),[3] spin-charge separation,[4] and valence-ordering states[5] in addition to the many advantages (e.g., a straightforward synthetic approach, easily tailored molecular structure and functional properties) of the organic component.

Bis-1,2-dithiolene complexes of transition metals have been widely studied because of their novel properties in the areas of magnetic[6] and conducting[7] materials. In our present studies, we focused on the assembly of quasi-1-D $S = {}^1/_2$ spin systems, which have been based on the molecular architectures of bis(maleonitriledithiolato)metalate monoanions ($[M(mnt)_2]^-$ and M = Ni, Pd, or Pt). To achieve such types of quasi-1-D magnetic molecular solids, a critical issue has been the control of the $[M(mnt)_2]^-$ anions in the columnar arrangement. The crystal packing mode of an inorganic salt, where the simple inorganic ions could be considered as point electric charges, and the electrostatic interactions between the pairs of point electric charges obey Coulomb's law, dependent mostly upon the Madelung energy (ionic lattice energy), while the arrangements of organic ions in an organic or inorganic−organic hybrid crystal were determined not only by the Madelung energy but also by the Lennard-Jones potential (which depended on molecular properties, such as the shape, size, polarity, local charge distribution, types and location of the functional groups of the molecules, which were generally less important than the Madelung energy). The behavior of the packing structure for planar paramagnetic $[M(mnt)_2]^-$ (M = Ni, Pd, or Pt) monoanions was strongly affected by the type of counterions;[8] for instance, a mixed stack was favorably formed when the $[M(mnt)_2]^-$ (M = Ni, Pd, or Pt) monoanions were combined with the planar monovalent countercations.[9] In earlier studies, we designed Λ-shape 1-*N*-benzylpyridinium derivatives as the counterions of $[M(mnt)_2]^-$ (M = Ni, Pd, or Pt) monoanions, which could prevent the anion (A) and cation (C) from forming a mixed stack arranged in the alternating ACAC manner, and we obtained a series of compounds with segregated anion and cation stacks; each $[M(mnt)_2]^-$ (M = Ni, Pd, or Pt) monoanion stack behaved as an $S = {}^1/_2$ spin chain. Therefore, it was reasonable to consider such an ion-pair compound as a quasi-1-D spin system. We noted that (1) the anions and cations showed a regular arrangement in some $[M(mnt)_2]^-$ compounds and irregular alignment in others within a stack, and

Received: December 2, 2010
Published: April 04, 2011

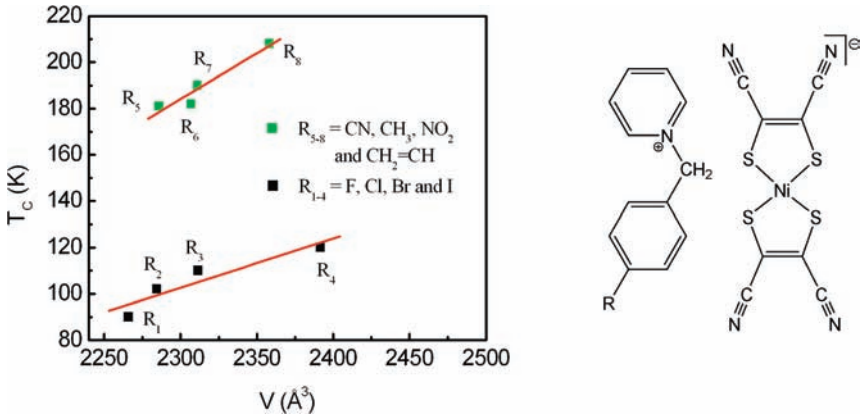

Figure 1. Correlation between spin-Peierls-type transition temperature T_C and cell volume V for the series of [4′-R-BzPy][Ni(mnt)$_2$] compounds (where 4′-R-BzPy$^+$ = the monosubstituted benzylpyridinium derivatives and the substituent located in the para-position of the phenyl ring).[8]

most compounds with regular anion and cation stacks as well as only a few compounds with the irregular anion and cation stacks exhibited a novel spin-Peierls-type transition below a critical temperature; (2) a correlation seemed to exist between the stacking pattern of the neighboring cations in a stack and the spin-Peierls-type transition; most of the compounds, which possessed a boat-type arrangement between the neighboring cations, showed the regular columnar stacks for both anions and cations and a spin-Peierls-type transition; (3) the local structural fluctuation, which is a common phenomenon in 1-D conductors and magnets and arises from electron−phonon or magnetoelastic coupling interactions, was observed with the spin-Peierls-type transition; (4) most of the spin-Peierls-type transitions were associated with a structural transition and the nonzero transition enthalpy; (5) the correlation between the characteristics of the substituent groups attached to the phenyl ring of the cation and the spin-Peierls-type transition temperature T_C was observed in some instances. The variation of T_C was independent of the electronic effect of the substituent in the series of [1-*N*-(4′-R-benzyl)pyridinium][Ni(mnt)$_2$] (R = F, Cl, Br, I, NO_2, CN, CH_3, and $CH{=}CH_2$). For example, the electron affinity of the substituent should follow the order: NO_2, CN > F > Cl > Br > I > $CH{=}CH_2$ > CH_3; whereas the variation of T_C in this family did not show this simple order. NO_2 and CH_3 possessed different electron donating and withdrawing effects, but the corresponding compounds had a similar transition temperature. As demonstrated in Figure 1, the variation of T_C appeared to be dependent on the size of the substituent group because the spin-Peierls-type transition temperature increased with the cell volume of the crystal, which increased with the atomic sizes and atomic numbers of the substituent located in the para-position of the phenyl ring.[8,10−12]

To understand the above-mentioned issues and establish the general validity of the correlation between the structural features of the countercation and the arranging pattern of the cationic stack column as well as the relationship between the arranging pattern of cationic stack column and the feature of the spin-Peierls-type transition, we sought to systematically investigate the crystal structures and magnetic behaviors for the series of [M(mnt)$_2$]$^-$ (M = Ni, Pd, and Pt) with benzylpyridinium derivatives. In this paper, the crystal structures and magnetic properties were studied for three ion-pair compounds of [Pt(mnt)$_2$]$^-$ with disubstituted benzylpyridinium derivatives, 4′-R-Bz-NH_2Py$^+$ (ref Scheme 1).

Scheme 1. Molecular Structures of Compounds 1−3

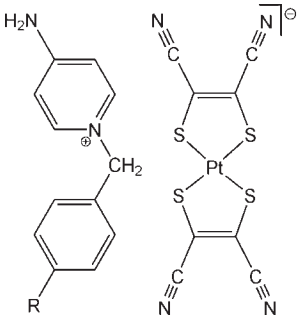

R	Complex
CN	(**1**)
Cl	(**2**)
H	(**3**)

EXPERIMENTAL SECTION

Chemicals and Materials. All reagents and chemicals were purchased from commercial sources and used without further purification. The starting materials, disodium maleonitriledithiolate (Na_2mnt),[13] 1-*N*-(4′-cyanobenzyl)-4-aminopyridinium bromide ([4′-CN-Bz-NH_2Py]Br), 1-*N*-(4′-chlorobenzyl)-4-aminopyridinium bromide ([4′-Cl-Bz-NH_2Py]Br), and 1-*N*-benzyl-4-aminopyridinium bromide ([Bz-NH_2Py]Br),[14] were prepared following the published procedures. [4′-CN-Bz-NH_2Py]$_2$[Pt(mnt)$_2$], [4′-Cl-Bz-NH_2Py]$_2$-[Pt(mnt)$_2$], and [Bz-NH_2Py]$_2$[Pt(mnt)$_2$] were synthesized utilizing a procedure similar to the preparation of [TBA]$_2$[Pt(mnt)$_2$].[13]

Syntheses of Compounds. *[4′-CN-Bz-NH_2Py][Pt(mnt)$_2$]·MeCN (**1**·MeCN).* A MeCN solution (10 mL) of I_2 (150 mg, 0.59 mmol) was slowly added to a MeCN solution (10 mL) of [4′-CN-Bz-NH_2Py]$_2$[Pt(mnt)$_2$] (896 mg, 1.0 mmol); the mixture was stirred for 20 min, and MeOH (80 mL) was then added. The mixture was allowed to stand overnight; the 548 mg of microcrystals that formed were filtered off, washed with MeOH, and dried in vacuum (∼80% yield). Single crystals of **1**·MeCN that were suitable for X-ray structure analysis were obtained by slowly evaporating the solution of **1** in MeCN at room temperature for 6 days. The analytical calculations for $C_{21}H_{12}N_7PtS_4 \cdot C_2H_3N$ included the following values: C, 38.01; H, 2.08; N, 15.42%. The experimental values found for this compound were the following: C, 37.37; H, 2.58; N, 14.61% (these values were close to the calculations based on the formula of $C_{21}H_{12}N_7PtS_4 \cdot 0.5C_2H_3N$: C, 37.40; H, 1.91; N, 14.88%). The peaks in the infrared (IR) spectrum (KBr disk, cm^{-1}) were found at the following values: 3442(s), 3342(s), 3238(s) for the ν_{N-H} of -NH_2; 3097(w), 3066(m) for the ν_{C-H} of the phenyl and pyridyl rings; 2208(vs) for the $\nu_{C\equiv N}$ of the mnt^{2-} ligands and the $\nu_{C\equiv N}$ of 4′-CN-Bz-NH_2Py$^+$; 1658(vs)

dx.doi.org/10.1021/ic102406u |*Inorg. Chem.* 2011, 50, 3970–3980

Table 1. Crystal and Structural Refinement Data for 1·MeCN, 2, and 3

	1·MeCN	2	3
chemical formula	$C_{23}H_{15}N_8PtS_4$	$C_{20}H_{12}ClN_6PtS_4$	$C_{20}H_{13}N_6PtS_4$
formula weight	726.79	695.17	660.72
CCDC number	CCDC 781810	CCDC 776573	CCDC 777239
temp./K	293(2)	296(2)	296(2)
wavelength/Å	0.71073	0.71073	0.71073
space group	$P2(1)/c$	$P2(1)/c$	$P\bar{1}$
a/Å	12.404(3)	7.3903(8)	11.533(4)
b/Å	31.060(7)	26.318(3)	14.191(5)
c/Å	7.2419(17)	12.7696(15)	15.786(5)
α/deg	90.00	90.00	73.318(7)
β/deg	105.571(4)	105.945(2)	74.034(7)
γ/deg	90.00	90.00	68.030(6)
V/Å^3, Z	2687.7(11), 4	2388.1(5), 4	2253.9(13), 4
Density(calc)/g·cm^{-3}	1.796	1.931	1.947
Abs. Coeff. (mm^{-1})	5.560	6.358	6.600
F(000)	1404.0	1328	1268
θ ranges of data collection	1.83−24.99	1.83−27.0	1.58−26.0
index ranges	$-8 \le h \le 14$	$-7 \le h \le 9$	$-14 \le h \le 12$
	$-35 \le k \le 36$	$-33 \le k \le 32$	$-16 \le k \le 17$
	$-8 \le l \le 8$	$-16 \le l \le 14$	$-19 \le l \le 11$
reflections collected	13023	15094	13172
R_{int}	0.0379	0.0399	0.1213
independent reflections	4672	5160	8622
refinement method on F^2	full-matrix least-squares		
goodness-of-fit on F^2	1.026	0.999	0.884
final R indices $[I > 2\sigma(I)]$	R_1 = 0.0983	R_1 = 0.0341	R_1 = 0.0396
	wR_2 = 0.2493	wR_2 = 0.0999	wR_2 = 0.0825
R indices (all data)	R_1 = 0.1219	R_1 = 0.0519	R_1 = 0.0754
	wR_2 = 0.2618	wR_2 = 0.1383	wR_2 = 0.0926
residual (e Å^{-3})	2.849/ −3.275	1.014/ −1.642	1.308/ −1.803

$R_1 = \Sigma||F_o| - |F_c||/\Sigma|F_o|$, $wR_2 = [\Sigma w(F_o^2 - F_c^2)^2/\Sigma w(F_o^2)^2]^{1/2}$.

for the $\nu_{C\equiv N}$ of the pyridyl ring and the $\nu_{C=C}$ of the phenyl ring; 1442(m) for the $\nu_{C=C}$ of mnt^{2-} ligands.

For the preparation of **2** and **3** similar procedures were used, but $[4'$-CN-Bz-$NH_2Py]_2[Pt(mnt)_2]$ was replaced with the corresponding salts of the benzylpyridinium derivative with the $[Pt(mnt)_2]^{2-}$ dianion.

[4′-Cl-Bz-NH_2Py][Pt(mnt)$_2$] (**2**). The product yield was ∼78%. The analytical calculations for $C_{20}H_{12}ClN_6PtS_4$ were the following: C, 34.56; H, 1.74; N, 12.09%. The experimental values included the following: C, 34.30; H, 1.88; N, 12.31%. The IR spectrum (KBr disk, cm^{-1}) showed peaks at the following values: 3477(s), 3373(vs), 3238(w) for the ν_{N-H} of -NH_2; 3099(w), 3072(w) for the ν_{C-H} of the phenyl and pyridyl rings; 2206(s) for the $\nu_{C\equiv N}$ of mnt^{2-} ligands; 1649(vs) for the $\nu_{C=N}$ of the pyridyl ring and the $\nu_{C=C}$ of the phenyl ring; 1452(s) for the $\nu_{C=C}$ of mnt^{2-} ligands.

[Bz-NH_2Py][Pt(mnt)$_2$] (**3**). The product yield was ∼82%. The analytical calculations for $C_{20}H_{13}N_6PtS_4$ were the following: C, 36.36; H, 1.98; N, 12.72%. The experimental values included the following: C, 36.22; H, 2.067; N, 12.72%. The IR spectrum (KBr disk, cm^{-1}) showed peaks at the following values: 3435(s), 3348(s), 3247(s) for the ν_{N-H} of -NH_2; 3099(w), 3066(s), 2976(w) for the ν_{C-H} of the phenyl and pyridyl rings; 2206(s) for the $\nu_{C\equiv N}$ of mnt^{2-} ligands; 1652(vs) for the $\nu_{C=N}$ of the pyridyl ring and the $\nu_{C=C}$ of the phenyl ring; 1446(s) for the $\nu_{C=C}$ of mnt^{2-} ligands.

Scheme 2. Illustration for the Characteristic Intermolecular Distances in a Tetrameric Subunit of 4′-CN-Bz-NH_2Py^+ Cations[a]

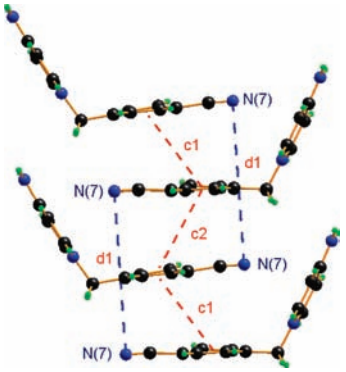

[a] d_1 is the distance of the N···N of the CN groups; c_1 and c_2 represent the centroid-to-centroid distances of the phenyl rings.

Single crystals of **2** and **3** that were suitable for X-ray structure analysis were obtained by slowly evaporating the solution with the corresponding compounds in MeCN at room temperature for 6−8 days.

Physical Measurements. Elemental analyses (C, H, and N) were performed with an Elementar Vario EL III analytical instrument. IR spectra were recorded on a Bruker Vector 22 Fourier Transform Infrared Spectrometer (170SX) (KBr disk). Magnetic susceptibility data for polycrystalline samples were measured over a temperature range of 1.8−300 K using a Quantum Design MPMS-5S superconducting quantum interference device (SQUID) magnetometer.

X-ray Single Crystallography. The single-crystal X-ray diffraction data for **1**·MeCN, **2** and **3** were collected at 296 K with graphite monochromated Mo Kα (λ = 0.71073 Å) on a CCD area detector (Bruker-SMART). Data reductions and absorption corrections were performed with the SAINT and SADABS software packages, respectively.[15] Structures were solved by a direct method using the SHELXL-97 software package.[16] The non-hydrogen atoms were anisotropically refined using the full-matrix least-squares method on F^2. All hydrogen atoms were placed at the calculated positions and refined riding on the parent atoms. The details about data collection, structure refinement and crystallography are summarized in Table 1.

DFT Calculations. All density functional theory (DFT) calculations were carried out using the Gaussan98 program[17] on an SGI 3800 workstation. The dipole moments of the cations, 4′-CN-Bz-NH_2Py^+ and 4′-Cl-Bz-NH_2Py^+, were calculated at the b3lyp/6-31g+(d,p) level[18] on the non-modelized molecular geometries, which were directly taken from the single crystal X-ray analyses. The single-point energies of the 4′-CN-Bz-NH_2Py^+ tetramers were calculated at the b3lyp/6-31g+(d,p) level for the regular and dimerized stacks. For these calculations, the molecular geometry for each 4′-CN-Bz-NH_2Py^+ cation in the tetrameric subunit was directly taken from the single crystal X-ray analysis, and the positions of four 4′-CN-Bz-NH_2Py^+ cations were not changed for the case of the regular cation stack, while the positions of two terminal cations were kept fixed and two central cations were translated to two opposite terminal cations along the N(7)···N(7) direction for the case of the dimerized stack; each case was identified by the characteristic intermolecular separations (ref Scheme 2). All SCF convergence criteria for DFT calculations were 10^{-8}.

dx.doi.org/10.1021/ic102406u |*Inorg. Chem.* 2011, 50, 3970–3980

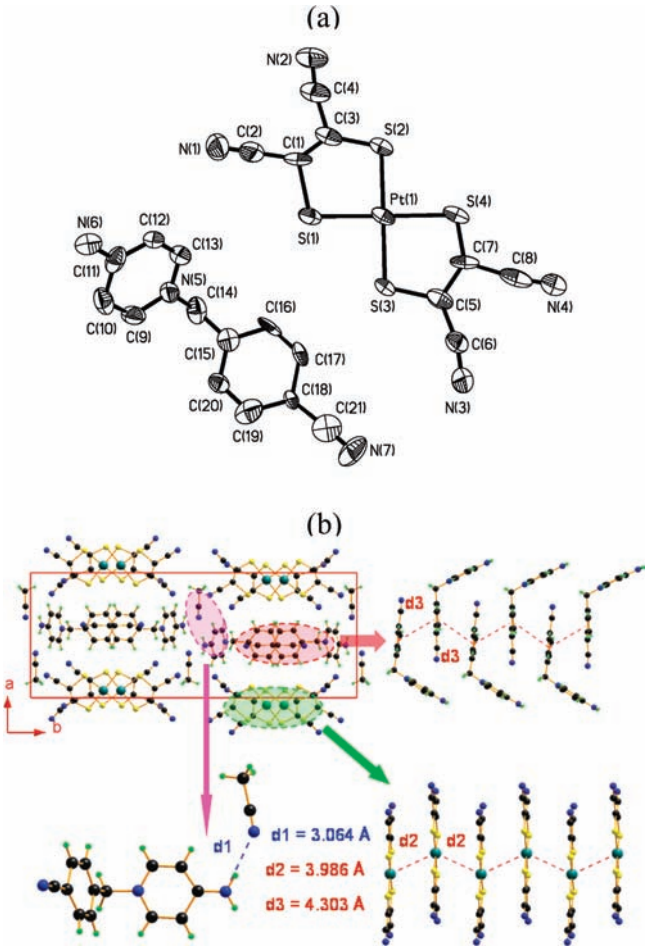

Figure 2. (a) ORTEP view with non-hydrogen atomic numbering at 30% thermal ellipsoid probability level; (b) packing diagram showing the segregated and regular stacks of anions and cations along the crystallographic *c*-axis direction as well as the hydrogen bond between the cation and the solvent acetonitrile for **1**·MeCN.

RESULTS AND DISCUSSION

Description of Crystal Structures. Compound **1**·MeCN crystallized in a monoclinic space group $P2(1)/c$. As shown in Figure 2a, an asymmetric unit comprised one $[Pt(mnt)_2]^-$ monoanion, explicitly one 4′-CN-Bz-NH_2Py^+ cation together with a MeCN molecule. In the $[Pt(mnt)_2]^-$ moiety, the Pt-atom was coordinated to four sulfur atoms from two mnt^{2-} ligands, exhibiting a square planar coordination geometry. The average distance of Pt−S bonds was 2.26 Å, and the average S−Pt−S bite angle was 90.45°; the other bond lengths and bond angles, listed in Table 2, were comparable to those of the reported $[Pt(mnt)_2]^-$ compounds.[11a] The 4′-CN-Bz-NH_2Py^+ cation adopted a Λ-shape conformation where the bond lengths and bond angles were normal, and both pyridyl and phenyl rings were twisted to the $C_{Bz}-C-N_{Py}$ reference plane with the corresponding dihedral angles 91.91° and 83.30°.

The anions and cations in **1**·MeCN formed regular stacks along the crystallographic *c*-axis direction (Figure 2b). Within an anion stack, the neighboring $[Pt(mnt)_2]^-$ anions were arranged in a rotational manner with an angle of 167.97° between their long molecular axes, the Pt···Pt distance of 3.986 Å, and the nearest S···S and Pt···S contacts of 3.794 and 3.785 Å. These

Table 2. Characteristic Bond Lengths and Angles in the $[Pt(mnt)_2]^-$ Moiety of 1·MeCN, 2, and 3

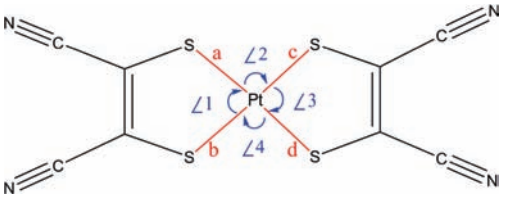

	1·MeCN	2	3*	
a/Å	2.272(6)	2.2717(18)	2.290(2)	2.2730(19)
b/Å	2.259(5)	2.2608(18)	2.282(2)	2.2803(19)
c/Å	2.235(5)	2.2740(18)	2.277(2)	2.2864(19)
d/Å	2.262(6)	2.2589(19)	2.280(2)	2.2675(19)
∠1/deg	89.8(2)	89.90(6)	90.00(7)	90.13(7)
∠2/deg	90.0(2)	91.90(7)	90.43(7)	90.09(7)
∠3/deg	90.10(18)	88.47(7)	89.67(7)	89.99(7)
∠4/deg	90.20(17)	89.74(7)	89.86(7)	89.81(7)

*There were two crystallographically different $[Pt(mnt)_2]^-$ anions in **3**.

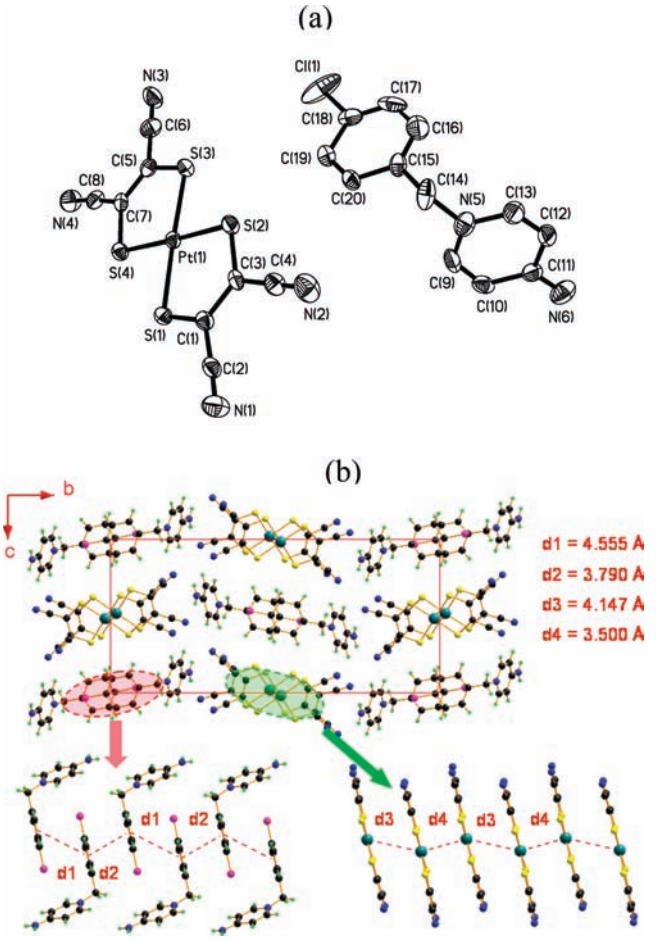

Figure 3. (a) ORTEP view with non-hydrogen atomic numbering at 30% thermal ellipsoid probability level; (b) packing diagram that shows the segregated and irregular stacks of anions and cations along the crystallographic *c*-axis direction for **2**.

dx.doi.org/10.1021/ic102406u |*Inorg. Chem.* 2011, 50, 3970–3980

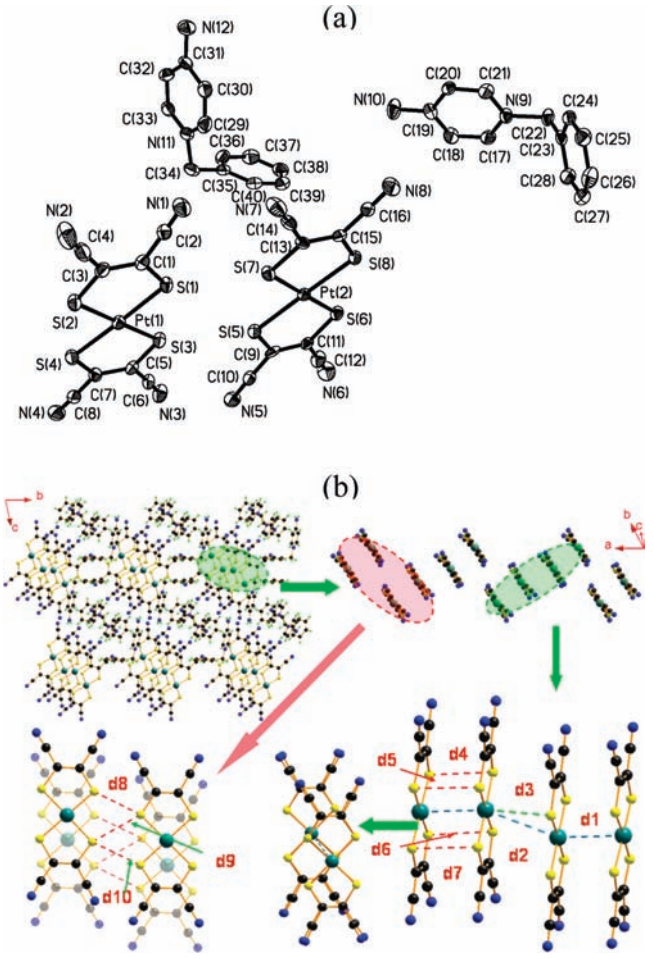

Figure 4. (a) ORTEP view with non-hydrogen atomic numbering at 30% thermal ellipsoid probability level; (b) packing diagram that shows a 1-D arrangement of anions with a tetramer subunit along the crystallographic *a*-axis direction as well as the shorter S···S, S···Pt and Pt···Pt distances (d_1 = 3.586, d_2 = 4.066, d_3 = 3.717, d_4 = 3.513, d_5 = 3.535, d_6 = 3.587, d_7 = 3.612, d_8 = 3.844, d_9 = 3.587, and d_{10} = 3.802 Å) within the 1-D tetrameric arrangement for **3**.

interatomic separations were slightly longer than the sums of the van der Waals radii of the corresponding atoms.[19] Within a cation stack, the adjacent Λ-shape cations adopted the boat-type arrangement, the phenyl rings of neighboring benzyl moieties were almost parallel to each other with a dihedral angle of 4.79° and the CN groups were superimposed on the phenyl rings with 3.462 and 3.413 Å as the shortest distances of the C and N atoms, respectively, to the mean molecular plane of the phenyl ring. The anion and cation stacks were arrayed into two-dimensional (2-D) molecular sheets that were parallel to the crystallographic *bc*-plane. In an anion sheet, the closest Pt···Pt separation between the anion stacks was 12.068 Å along the crystallographic *b*-axis direction; this distance was significantly longer than that of the Pt···Pt separation within a stack. Therefore, from the structural viewpoint, **1**·MeCN could be considered a uniform chain spin system.

Compound **2** crystallized in a monoclinic space group $P2(1)/c$, and its asymmetric unit consisted of one pair of $[Pt(mnt)_2]^-$ and 4′-Cl-Bz-NH_2Py^+ ions, as shown in Figure 3a. The bond parameters in the planar $[Pt(mnt)_2]^-$ entry were comparable to those in **1**·MeCN, as listed in Table 2. The pyridyl and phenyl rings formed a dihedral angle of 108.45° and 72.39°, respectively, with the $C_{Bz}-C-N_{Py}$ reference plane in the Λ-shape 4′-Cl-Bz-NH_2Py^+ cation. These dihedral angles were larger than the corresponding values in 4′-CN-Bz-NH_2Py^+ of **1**·MeCN. The $[Pt(mnt)_2]^-$ and 4′-Cl-Bz-NH_2Py^+ stacks ran parallel to the crystallographic *a*-axis direction, with each stack flanked by four stacks of opposite charge (ref Figure 3b). Such an arrangement was obviously different from that in **1**·MeCN.

In an anion stack, two neighboring $[Pt(mnt)_2]^-$ anions formed the eclipsed π-type $[Pt(mnt)_2]_2^{2-}$ dimer with an intradimer separation of $d_{plane\text{-}to\text{-}plane}$ = 3.520 Å (the mean-molecular plane of $[Pt(mnt)_2]^-$ anion was defined by four S atoms), $d_{Pt1\cdots Pt\#1}$ = 3.500 Å, $d_{S1\cdots S3\#1}$ = 3.564 Å, $d_{S2\cdots S4\#1}$ = 3.486 Å (symmetric code: #1 = 2 − *x*, 1 − *y*, −*z*). As shown in Figure 3b, the slippages occurred between the adjacent $[Pt(mnt)_2]_2^{2-}$ dimers along both the long and the short molecular axes; the interdimer plane-to-plane separation was 3.669 Å, the interdimer Pt···Pt distance was 4.147 Å, and the nearest interdimer S···S and Pt···S contacts were 3.962 and 3.825 Å, respectively. In a 4′-Cl-Bz-NH_2Py^+ stack, two adjacent cations arranged in a chair-type fashion to form a cationic dimer (Figure 3b). The phenyl rings in the benzyl moieties were parallel to each other, owing to the geometric constraint by an inversion center, and the interplane distance between the parallel phenyl rings was 3.502 Å within a cationic dimer and 3.512 Å between the cationic dimers.

The crystal of **3** belonged to a triclinic system with space group $P\bar{1}$ and was isomorphic with its analogue [Bz-NH_2Py][Ni(mnt)$_2$].[14] The asymmetric unit depicted in Figure 4a contained two pairs of $[Pt(mnt)_2]^-$ and Bz-NH_2Py^+ ions. Two crystallographically different planar anions were almost parallel to each other (two mean molecular planes defined by four S atoms formed a dihedral angle of 1.62° and built an angle of 17.82° for the Pt(1)-anion versus 16.75° for the Pt(2)-anion with the crystallographic *bc*-plane). The geometric parameters in two crystallographically different $[Pt(mnt)_2]^-$ anions were normal and in agreement with those in **1**·MeCN and **2** (ref Table 3). The dihedral angles between pyridyl and phenyl rings and the $C_{Bz}-C-N_{Py}$ reference plane were distinct in two crystallographically independent Λ-shape Bz-NH_2Py^+ cations; these angles were 103.5° and 89.6° in one cation and 92.9° and 80.2° in another cation. As illustrated in Figure 4b, the $[Pt(mnt)_2]^-$ anions formed a tetrameric subunit in which two types of crystallographic anions were arranged in a manner of Pt(1)Pt(2)Pt(2)Pt(1), where a terminal Pt(1) anion and a central Pt(2) anion stacked into an eclipsed π-type $[Pt(mnt)_2]_2^{2-}$ dimer with an intradimer plane-to-plane separation of 3.514 Å (the mean-molecular plane of the $[Pt(mnt)_2]^-$ anion was defined by four S atoms), Pt···Pt separation of d_1 = 3.586 Å, S···S contacts of d_4 = 3.513, d_5 = 3.535, d_6 = 3.587, and d_7 = 3.612 Å; two dimers in a tetrameric subunit slipped along a Pt−S bond direction, leading to an increase of Pt···Pt separation (d_2 = 4.066 Å) and a decrease of Pt···S distance (d_3 = 3.717 Å). The adjacent tetrameric subunits were connected into a zigzag-type stack via weakly lateral S···S contacts (with the shorter S···S separations of d_8 = 3.844, d_9 = 3.587, and d_{10} = 3.802 Å) along the crystallographic *a*-axis direction. It was noted that the structure of **3** was remarkably different from that of **1**·MeCN and **2**. First, the cations filled the space between the tetrameric anion stacks but did not form a cofacial stack. Second, strong intermolecular H-bond interactions were formed between the CN groups of the

dx.doi.org/10.1021/ic102406u |*Inorg. Chem.* 2011, 50, 3970–3980

Table 3. Stacking Manner of Cations and Spin-Peierls-Type Transition in Reported Compounds

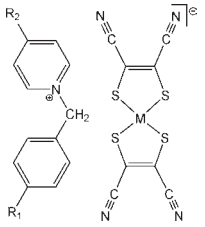

substituents						
R1	R2	M	stacking manner of cations	stacking manner of anions	SP transition	ref.
F	H	Ni	boat-type	regular stack	$T_C \approx 90$ K	10b
Cl	H	Ni	boat-type	regular stack	$T_C \approx 102$ K	10a
Br	H	Ni	boat-type	regular stack	$T_C \approx 110$ K	10a
I	H	Ni	boat-type	regular stack	$T_C \approx 120$ K	10e
NO_2	H	Ni	boat-type	regular stack	$T_C \approx 181$ K	10a
CH_3	H	Ni	boat-type	regular stack	$T_C \approx 182$ K	10f
CN	H	Ni	boat-type	regular stack	$T_C \approx 190$ K	10c
$CHCH_2$	H	Ni	boat-type	regular stack	$T_C \approx 208$ K	10d
F	H	Pd	chair-type	irregular stack	no	11c
Cl	H	Pd	chair-type	irregular stack	no	11b
Br	H	Pd	chair-type	irregular stack	no	11b
I	H	Pd	chair-type	irregular stack	no	11b
NO_2	H	Pd	chair-type	irregular stack	no	11b
Cl	H	Pt	boat-type	regular stack	$T_C \approx 275$ K	11a
Br	H	Pt	boat-type	regular stack	$T_C \approx 269$ K	11a
I	H	Pt	chair-type	irregular stack	$T_C \approx 80$ K	11d
NO_2	H	Pt	chair-type	irregular stack	$T_C \approx 184$ K	11a
CN[a]	H	Pt	boat-type	regular stack	no	12a
F[b]	NH_2	Ni	boat-type	regular stack	no	12b
Cl	NH_2	Ni	boat-type	regular stack	$T_C \approx 87$ K	12c
Br	NH_2	Ni	boat-type	regular stack	$T_C \approx 105$ K	12d
I	NH_2	Ni	boat-type	regular stack	no	12e
NO_2	NH_2	Ni	boat-type	regular stack	$T_C \approx 160$ K	12f
CN	NH_2	Ni	boat-type	regular stack	$T_C \approx 210$ K	12g
CH_3	NH_2	Ni	boat-type	regular stack	$T_C \approx 155$ K	10f
Cl	NH_2	Pt	chair-type	irregular stack	no	this work
CN	NH_2	Pt	boat-type	regular stack	$T_C \approx 240$ K	this work

[a] There was a larger slippage between the neighboring anions along the shorter molecular axis in an anion stack, and the neighboring phenyl rings did not form a face-to-face overlap in the cation stack. [b] The neighboring pyridyl rings in this compound and the phenyl rings in others were superimposed within a cation stack.

Pt(2)-anions and the NH_2 groups in the N(12)-cation moieties, which gave rise to a 2 + 2 H-bond supramolecular ring (two anions with two cations, as shown in Figure 5).

Magnetic Properties. The temperature-dependent magnetic susceptibility of **1**·MeCN, with both χ_m and $1/\chi_m$, formed at 1.8−300 K is displayed in Figure 6, where χ_m represents the molar magnetic susceptibility corresponding to one $[Pt(mnt)_2]^-$ anion per formula unit, and the diamagnetic correction was not made. From the plots, it could be determined that a spin-Peierls-type transition occurred at around 240 K, and no sizable hysteresis loop was detected in the cooling and heating procedures. Below 240 K, a spin gap opened in the magnetic excitation spectrum, which separated the nonmagnetic ground state from a continuum of magnetically excited states. Theoretically, the paramagnetic susceptibility should become zero as the temperature decreases below the spin-Peierls-type transition; however, a Curie-type paramagnetic behavior was observed in the low-temperature region, which was attributed to magnetic impurity (due to, for example, a lattice defect). As a consequence, the variable-temperature magnetic susceptibility in the low-temperature phase could be fitted using eq 1,

$$\chi_m = \frac{C}{T} + \chi_0 \quad (1)$$

where χ_0 is contributed by the core diamagnetism and the possible van Vleck paramagnetism, and the C/T term represents the paramagnetism from the magnetic impurity. The best fit was obtained in the temperature region of 1.8−120 K, which gave rise

dx.doi.org/10.1021/ic102406u |*Inorg. Chem.* 2011, 50, 3970–3980

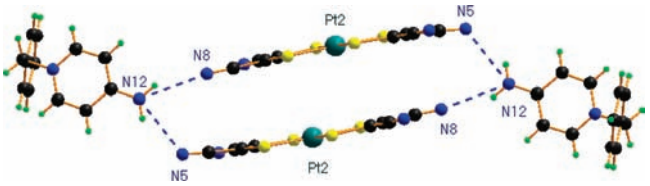

Figure 5. Bifurcated hydrogen bond interactions between NH_2 groups in N(12)-cation moieties and CN groups of Pt(2)-anions with geometric parameters of $d_{N(12)\cdots N(5)\#1}$ = 3.018 Å, ∠N(12)−H(12B)···N(5)#1 = 137.51° and $d_{N(12)\cdots N(5)\#2}$ = 3.108 Å, ∠N(12)−H(12A)···N(5)#1 = 150.82° (symmetric codes: #1 = x, y, $1 + z$ and #2 = $2 - x$, $1 - y$, $1 - z$).

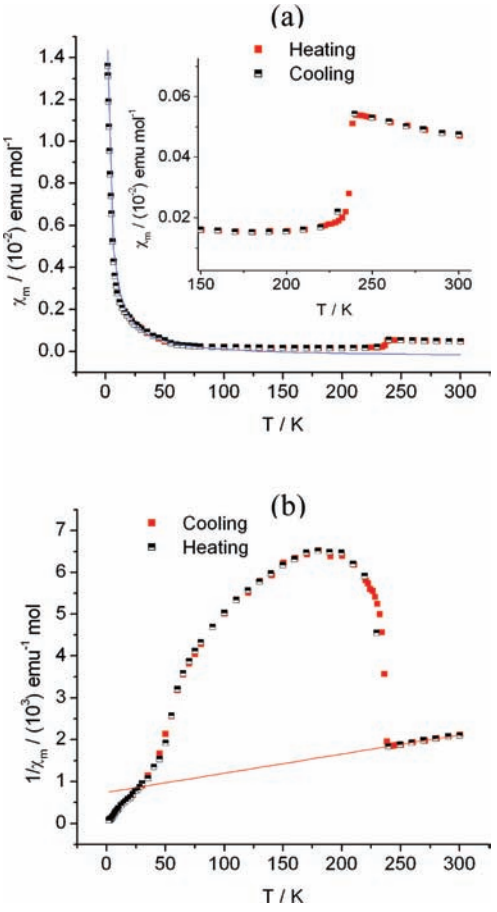

Figure 6. Plots of (a) χ_m vs T in both heating and cooling procedures (blue line represents the fit using eq 1 in the temperature range of 2−120 K) (b) $1/\chi_m$ vs T (red line is the fit using the Curie−Weiss law in the temperature range of 240−300 K) for **1**·MeCN.

to C = 0.04 emu·K·mol^{-1}, $\chi_0 = -3.0 \times 10^{-4}$ emu·mol^{-1}, and this diamagnetic susceptibility agreed well with the experimental value for the diamagnetic and isostructural $[Au(mnt)_2]^-$ compound (-2.9×10^{-4} emu·mol^{-1}).[20] To analyze the magnetic behavior in the high-temperature phase, the temperature-dependent magnetic susceptibility (in the temperature range of 240−300 K) was further fitted utilizing the Curie−Weiss law, and the corresponding parameters were estimated to be $C \approx$ 0.218 emu·K·mol^{-1} and $\theta \approx -161$ K, indicating that the antiferromagnetic coupling interactions dominated between the neighboring spins in the high-temperature phase.

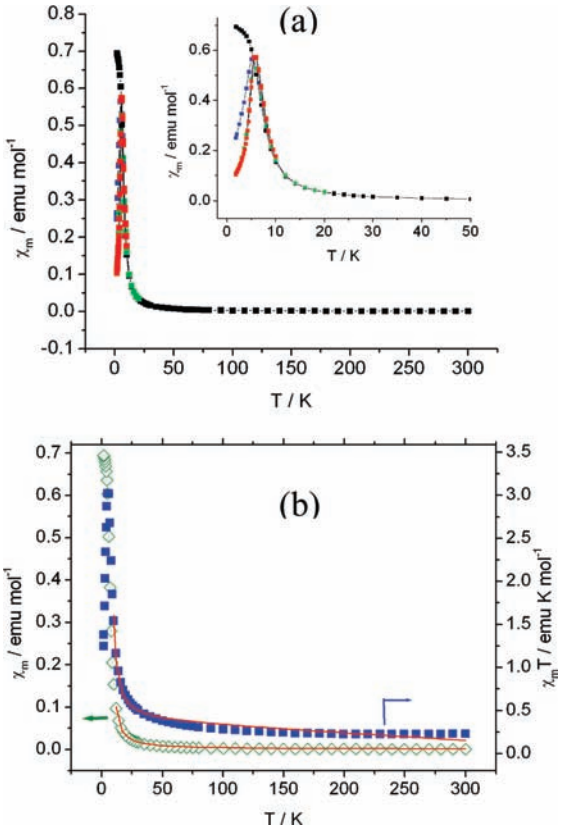

Figure 7. (a) plots of χ_m vs T (black, blue, red, and green solid squares represent the magnetic susceptibility data under the applied magnetic field of 2000 Oe, 1000 Oe, 500 and 10 Oe, respectively; (b) the plots of χ_m vs T and $\chi_m T$ vs T (under an applied field of 2000 Oe) and the theoretically produced plots in the range 9−300 K (red line) for **2**.

The variable-temperature magnetic susceptibilities were measured under different magnetic fields (10, 500, 1000, and 2000 Oe) for **2**; their plots of χ_m versus T are shown in Figure 7a, and the curve of $\chi_m T$ versus T under the applied magnetic field of 2000 Oe is illustrated in Figure 7b (where χ_m represents the corrected molar magnetic susceptibility, corresponding to one $[Pt(mnt)_2]^-$ anion per formula unit, and the molar diamagnetic susceptibility was approximately equal to that of the $[Au(mnt)_2]^-$ analogue, $\chi_d = -2.9 \times 10^{-4}$ emu·mol^{-1}).[20] The magnetic properties of **2** showed two characteristics: (1) the dominant magnetic coupling interactions in **2** were weakly ferromagnetic over the temperature range of 6−300 K and (2) the molar magnetic susceptibility was independent of the applied magnetic field above ∼6 K but dependent on the applied magnetic field below ∼6 K; a magnetic susceptibility maximum was observed at ∼6 K under lower applied magnetic fields, and this maximum disappeared when the applied magnetic field was greater than 1000 Oe. The variable-temperature alternating current (ac) magnetic susceptibility measurements were carried out, and the corresponding χ' versus T and χ'' versus T curves are illustrated in Figure 8a. A broad peak in the temperature range of 2.5−15 K, with a maximum around 5.8 K, appeared in the χ' versus T plot, indicating that the magnetic ordering may have occurred near this temperature, whereas no out-of-phase signal (χ'') was observed in the same temperature interval (i.e., there was no net magnetic moment in this magnetic ordering state). The magnetic field dependence of the magnetization was further

dx.doi.org/10.1021/ic102406u |*Inorg. Chem.* 2011, 50, 3970–3980

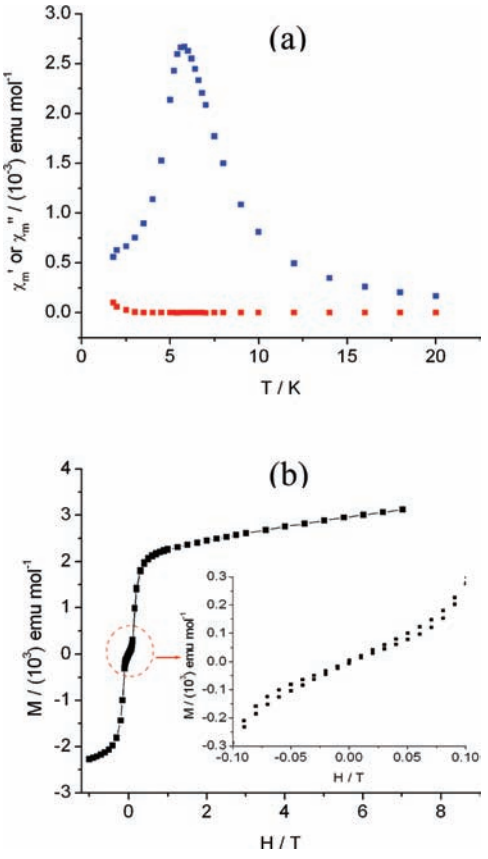

Figure 8. (a) ac magnetic susceptibility with $f = 10$ Hz and (b) M vs H plot for **2**.

measured at 1.8 K, as shown in Figure 8b. The M versus H plot exhibited an S-shape, a typical feature of metamagnetic behavior, with a small hysteresis loop. The critical magnetic field was estimated to be 1000 Oe from the peak in the dM/dH versus H curve (Supporting Information, Figure S2). These results suggest that **2** was an antiferromagnet with $T_N \approx 5.8$ K and metamagnetic behavior.

Antiferromagnets with a large anisotropy do not show a spin-flop phase but, in the presence of competing interactions, they may undergo a first-order transition to a phase in which there exists a net magnetic moment.[21] The choice of an appropriate magnetic model and the investigation of the magnetostructure correlations were helpful for understanding the metamagnetic behavior in **2**. Thus, we tried to fit the magnetic susceptibility data in the paramagnetic phase by utilizing different magnetic exchange models. From the viewpoint of crystal structure, an irregular $[Pt(mnt)_2]^-$ stack in **2** could be considered an alternating 1-D $S = {}^1/_2$ chain or a dimer spin system. However, no analytical expression has yet been established for a ferromagnetic alternating chain of an $S = {}^1/_2$ system. Given the assumption that two magnetic exchange constants within an alternating chain are not so different from each other and the consideration of the $[Pt(mnt)_2]^-$ stack as a ferromagnetic uniform chain, the expression given in eq 2,

$$\chi_m = \frac{Ng^2\beta^2}{4k_BT} \cdot \left(\frac{A}{B}\right)^{2/3} \qquad (2)$$

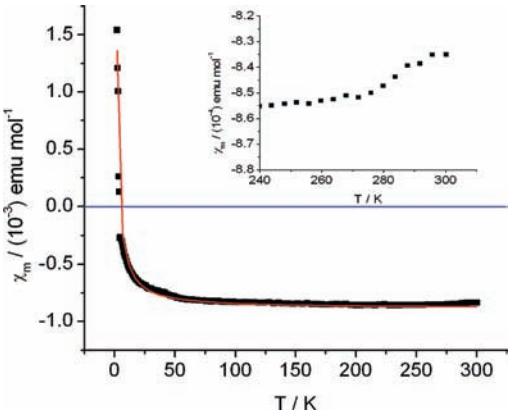

Figure 9. Plot of χ_m versus T for **3** (open circles: experimental data; red line: fitting in the temperature range of 1.8−200 K).

where $A = 1.0 + 5.7980x + 16.9027x^2 + 29.3769x^3 + 29.8329x^4 + 14.0369x^5$, $B = 1.0 + 2.7980x + 7.0087x^2 + 8.6538x^3 + 4.5743x^4$, and $x = J/2k_BT$, which was proposed by Baker and Rushbrooke[22] and derived from a high-temperature series expansion combined with a 2-D approach involving a "chain of chains"[23] was used in an attempt to fit the magnetic susceptibility data from room temperature to 9 K. However, the fit failed to offer reasonable parameters and to reproduce the experimental susceptibility curve (Supporting Information, Figure S3). This result suggested that the two magnetic exchange constants that corresponded to two alternating Pt···Pt distances within a $[Pt(mnt)_2]^-$ stack were significantly different. It was also noteworthy that the modified Blaney−Bowers equations, eq 3 and eq 4, were not able to provide reasonable results (where J and zJ' represent the magnetic exchange constants of intradimer and interdimer, respectively):

$$\chi_m = \frac{\chi_{dimer}}{1 - (zJ'/Ng^2\beta^2)\chi_{dimer}} \qquad (3)$$

$$\chi_{dimer} = \frac{Ng^2\beta^2}{k_BT} \cdot \left[3 + \exp\left(\frac{-2J}{k_BT}\right)\right]^{-1} \qquad (4)$$

Finally, we fitted the molar magnetic susceptibilities in the temperature region of 9−300 K for **2**, employing the simple Curie−Weiss law to produce the parameters $C \approx 0.387$ emu·K·mol^{-1} and $\theta \approx 8.1$ K (for the reproduced magnetic susceptibility curve, refer to Figure 7b). The fitted Curie constant was close to 0.375 emu·K·mol^{-1} (which was deduced from the spin-only magnetic moment with an $S = {}^1/_2$ spin system), and the small positive Weiss constant indicated the existence of dominant ferromagnetic coupling interactions in **2**. The peculiar metamagnetic behavior of **2** was caused by the competition between the relatively stronger ferromagnetic (FM) and the relatively weaker antiferromagnetic (AFM) coupling interactions. Two possibilities existed: (1) the existence of FM interactions in an intrastack and AFM interactions between the interstacks of $[Pt(mnt)_2]^-$ anions and (2) the occurrence of FM interactions within a $[Pt(mnt)_2]^-$ dimer of the anion stack and AFM interactions between $[Pt(mnt)_2]^-$ dimers. At present, these two types of magnetic exchange schemes can not be distinguished, and further theoretical investigation is needed.

For **3**, the molar magnetic susceptibility as a function of temperature, as illustrated in Figure 9, showed three striking

dx.doi.org/10.1021/ic102406u |Inorg. Chem. 2011, 50, 3970–3980

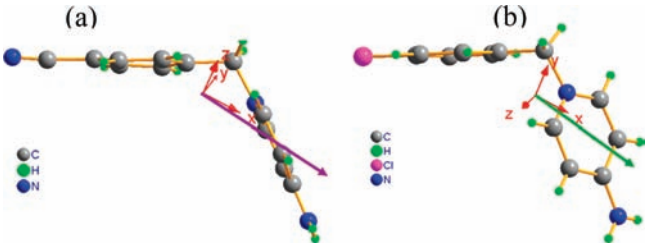

Figure 10. Cartesian coordinate system chosen for dipole moment calculations of (a) 4′-CN-Bz-NH_2Py^+ and (b) 4′-Cl-Bz-NH_2Py^+ (the magenta and olive arrows represent the calculated dipole vectors; the total dipole and its three components along the *X*, *Y* and *Z*-directions, respectively, were 14.5771, 14.5327, 0.7979, and 0.8101 D in 4′-CN-Bz-NH_2Py^+ versus 12.0502, 12.0419, 0.4243, and 0.1355 D in 4′-Cl-Bz-NH_2Py^+).

characteristics: the diamagnetism in the temperature range of 5−300 K, the weak paramagnetism below 5 K, and the magnetic susceptibility that slightly increased as the temperature rose in the higher-temperature region. The magnetic susceptibility data over the 1.8−200 K temperature range were further fitted to eq 1, giving rise to $C \approx 4.48 \times 10^{-3}$ emu·K·mol^{-1} and $\chi_0 \approx -8.9 \times 10^{-4}$ emu·mol^{-1}. These observations indicate the existence of a nonmagnetic ground state and a larger energy gap between the nonmagnetic ground state and the magnetic excited state. The crystal structure analysis for **3** disclosed that two crystallographically different $[Pt(mnt)_2]^-$ anions were arranged in the tetrameric stack, where a terminal anion and a central anion within a tetrameric unit stacked into an eclipsed π-type $[Pt(mnt)_2]_2^{2-}$ dimer with shorter intradimer separation and shorter interatomic distances. The strong AFM interaction that led to **3**, which showed almost diamagnetism in the temperature range of 5−300 K, was due to the large overlap of magnetic orbitals between the two eclipsed $[Pt(mnt)_2]^-$ monomers.[24]

Cation Arrangement Pattern in a Columnar Stack and Spin-Peierls-Type Transition. In recent studies, we have designed, synthesized, and characterized more than 30 compounds of planar $[M(mnt)_2]^-$ with Λ-shape 1-*N*-(4′-R_1-benzyl)-4-R_2-pyridinium derivatives (M = Ni, Pd, and Pt; R_2 = H or NH_2, as listed in Table 3); most of these compounds showed segregated stacks of anions and cations in the crystal structures. From the viewpoint of structure, these compounds could be divided into two main subgroups according to the manner in which they aligned with neighboring cations in a columnar stack. The compounds in which the neighboring cations adopted boat-type and chair-type configurations were classified as structural class I and II, respectively. In structural class I, all compounds exhibited regular stacks for both anions and cations, and most of the compounds displayed a spin-Peierls-type transition below a critical temperature. In structural class II, all compounds had irregular stacks for both anions and cations; only two compounds showed a spin-Peierls-type transition. Thus, there was probably an intrinsic relationship between the spin-Peierls-type transition and the stacking manner of the neighboring cations. This type of magnetic transition was generally associated with a structural dimerization of anion and cation stacks and the nonzero transition enthalpy, which was a typical characteristic of the first-order phase transition; however, the spin-Peierls transition was theoretically the second-order phase transition. As a result, it is obvious that some structural factors other than the magnetoelastic interactions also played an important role in the spin-Peierls-type magnetic transition for the $[M(mnt)_2]^-$ (M = Ni or Pt) compounds.

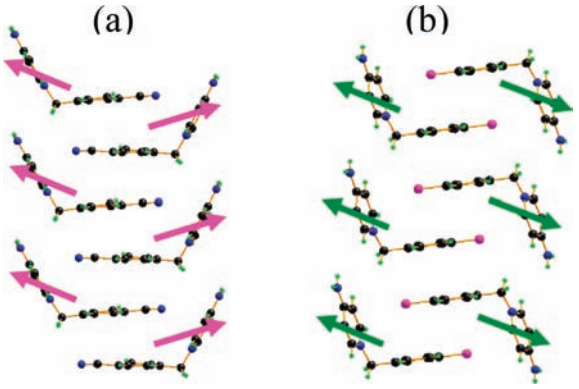

Figure 11. Schematic illustrations of dipole arrangements in a cationic stack for (a) **1**·MeCN (with the boat-type alignment between the neighboring cations) and (b) **2** (with the chair-type alignment between the neighboring cations).

Table 4. Relative Energy and the Characteristically Geometric Parameters (ref. Scheme 2) for a Tetrameric Subunit of 1-*N*-(4′-CN-benzyl)-4-aminopyridinium in 1·MeCN

	d1 (Å)	c1 (Å)	c2 (Å)	ΔE (kJ·mol^{-1})
regular stack	7.242	4.303	4.303	0.0
dimerized stack-1	7.300	4.255	4.401	−2.3103
dimerized stack-2	7.350	4.214	4.486	−2.9979
dimerized stack-3	7.400	4.172	4.572	+0.1930[a]

[a] Notes: the repulsive energy between two face-to-face phenyl rings increased when the terminal and the central cations were close to each other, which led to an increase in the energy of the dimerized stack.

To explore this issue, the dipole moments of a 4′-CN-Bz-NH_2Py^+ cation in **1**·MeCN and a 4′-Cl-Bz-NH_2Py^+ cation in **2** were calculated. The chosen Cartesian coordinate system, together with the calculated dipole vectors, is shown in Figure 10. The cationic stack showed different polarity in the cases of the neighboring cations adopted in the boat-type (structural class I) or chair-type (structural class II) arrangement. As illustrated in Figure 11, the dipole moments were canceled out between the neighboring cations in the 4′-Cl-Bz-NH_2Py^+ stack (structural class II) because they were related via an inversion center. There was a net dipole moment along the columnar direction in the 4′-CN-Bz-NH_2Py^+ stack (structural class I), and such a polar cation stack was highly energetically unfavorable, indicating the existence of structural strain in a boat-type cation stack. Furthermore, the single point energy for a tetrameric subunit of 4′-CN-Bz-NH_2Py^+ cations was calculated for the regular and dimerized stacks (ref Scheme 2). The results summarized in Table 4 revealed that the structural strains of the polar 4′-CN-Bz-NH_2Py^+ cation stack could be released via the dimerization.

In addition, we inspected all crystal structure data for the series of quasi-1-D [benzylpyridinium derivative][$M(mnt)_2$] compounds (M = Ni, Pd, and Pt) and found that the neighboring cations related by an inversion center were a common feature when the cation stack possessed a chair-type arrangement. These findings were helpful in understanding two issues for the series of quasi-1-D [benzylpyridinium derivative][$M(mnt)_2$] compounds: (1) the origin of the spin-Peierls-type transition, and (2) the

dx.doi.org/10.1021/ic102406u |*Inorg. Chem.* 2011, 50, 3970–3980

preference of the spin-Peierls-type transition for compounds with a boat-type cation arrangement.

CONCLUDING AND REMARKS

In summary, three ion-pair compounds of $[Pt(mnt)_2]^-$ monoanions with 1-*N*-(4′-CN-benzyl)-4-aminopyridinium derivatives were structurally and magnetically characterized. For **1**·MeCN, **2** and **3**, the substituent in the phenyl ring of the cation affected the packing structure of the ion-pair compounds. The anions and cations formed segregated columnar stacks in **1**·MeCN and **2**, while only the anions formed the zigzag-type stacks with a tetrameric $[Pt(mnt)_2]^-$ subunit and the cations filled the spaces between the anionic stacks in **3**. The cation and anion stacks were regular, and the neighboring 1-*N*-(4′-CN-benzyl)-4-aminopyridinium cations were arranged in the boat-type pattern within a stack for **1**·MeCN; in contrast, both cation and anion stacks were irregular and the neighboring 1-*N*-(4′-Cl-benzyl)-4-aminopyridinium cations were aligned in the chair-type manner within a stack for **2**. A spin-Peierls-type transition occurred around 240 K for **1**·MeCN; a long-range AFM ordering took place with T_N = 5.8 K, and below T_N, a peculiar metamagnetic phenomenon was observed with the critical field of ∼1000 Oe for **2**. The very strong AFM interactions within the tetramer $[Pt(mnt)_2]^-$ stack in **3** was due to the large overlap of magnetic orbitals between the two eclipsed $[Pt(mnt)_2]^-$ monomers. Therefore, compound **3** showed almost diamagnetism in the temperature range of 5−300 K.

In combination with our previous studies on the family of quasi-1-D magnetic compounds of [benzylpyridinium derivative]-$[M(mnt)_2]$ (M = Ni, Pd and Pt), the present findings reveal a correlation between the spin-Peierls-type transition and the stacking manner of the neighboring benzylpyridinium derivative cations; the compounds with the boat-type stacking pattern within a regular cation stack preferably elicited a spin-Peierls-type transition. Such a transition was probably driven by two factors acting together, including the magnetoelastic interaction between the magnetic $[M(mnt)_2]^-$ stacks and the lattice and the release of structural strains within the diamagnetic stacks of the benzylpyridinium derivative, as net dipole moments existed and the structural strains could be released via the dimerization of the stack in such a polar cation column.

A few open issues related to the stacking pattern of the cations and the nature of the molecular buildings (the electronic and geometric properties for both anions and cations) still remained in the series of quasi-1-D [benzylpyridinium derivative][M-$(mnt)_2$] compounds (M = Ni, Pd, and Pt). For example, all $[Pd(mnt)_2]^-$ compounds showed irregular stacks for both anions and cations, and the neighboring cations were aligned in the chair-type configuration within a stack; the same benzylpyridinium derivative cations were adopted in the boat-type configuration in $[Ni(mnt)_2]^-$ compounds, but in the chair-type pattern in the corresponding $[Pt(mnt)_2]^-$ compounds and vice versa. The question remains as to which factors played a critical role in the control of the stacking pattern of benzylpyridinium derivative cations. The research to establish the correlations between the factors not explained is in progress.

ASSOCIATED CONTENT

Supporting Information. Crystallographic data in CIF format for **1**·MeCN, **2**, and **3**, and the profiles of CN···π, Cl···π interactions in **1**·MeCN and **2**, and the reproduced magnetic susceptibility plots for **1**·MeCN and **2** in PDF format. This material is available free of charge via the Internet at http://pubs.acs.org.

AUTHOR INFORMATION

Corresponding Author

*Phone: +86 25 83587820. Fax: +86 25 83587438. E-mail: xmren@njut.edu.cn.

ACKNOWLEDGMENT

The authors thank the National Nature Science Foundation of China for their financial support (Grant 20871068 and 20901039), and X.-M.R. thanks Prof. C. J. Fang for reading the manuscript.

REFERENCES

(1) (a) Peierls, R. E. *Quantum Theory of Solids*; Clarendon Press: Oxford, U. K., 1955; pp 108−112; (b) Allen, S.; Piéri, J.-C.; Bourbonnais, C.; Poirier, M.; Matos, M.; Henriques, R. T. *Europhys. Lett.* **1995**, *32*, 663–668. (c) Ota, A.; Yamochi, H.; Saito, G. *J. Mater. Chem.* **2002**, *12*, 2600–2602.

(2) (a) Bray, J. W.; Hart, H. R.; Interrante, L. V., Jr.; Jacobs, I. S.; Kasper, J. S.; Watkins, G. D.; Wee, H.; Bonner, J. C. *Phys. Rev. Lett.* **1975**, *35*, 744. (b) Jacobs, I. S.; Bray, J. W.; Hart, H. R., Jr.; Interrante, L. V.; Kasper, J. S.; Watkins, G. D.; Prober, D. E.; Bonner, J. C. *Phys. Rev. B* **1976**, *14*, 3036. (c) Hase, M.; Terasaki, I.; Uchinokura, K. *Phys. Rev. Lett.* **1993**, *70*, 3651.

(3) (a) Coomber, A. T.; Beljonne, D.; Friend, R. H.; Brédas, J. L.; Charlton, A.; Robertson, N.; Underhill, A. E.; Kurmoo, M.; Day, P. *Nature* **1996**, *380*, 144–146. (b) Wei, J. H.; Zhao, J. Q.; Liu, D. S.; Xie, S. J.; Mei, L. M.; Hong, J. *Synth. Met.* **2001**, *122*, 305–309. (c) Takaishi, S.; Takamura, M.; Kajiwara, T.; Miyasaka, H.; Yamashita, M.; Iwata, M.; Matsuzaki, H.; Okamoto, H.; Tanaka, H.; Kuroda, S.-i.; Nishikawa, H.; Oshio, H.; Kato, K.; Takata, M. *J. Am. Chem. Soc.* **2008**, *130*, 12080–12084.

(4) Lorenz, T.; Hofmann, M.; Grüninger, M.; Freimuth, A.; Uhrig, G. S.; Dumm, M.; Dressel, M. *Nature* **2002**, *418*, 614–617.

(5) Mitsumi, M.; Kitamura, K.; Morinaga, A.; Ozawa, Y.; Kobayashi, M. *Angew. Chem., Int. Ed.* **2002**, *41*, 2767–2771.

(6) (a) Nihei, M.; Tahira, H.; Takahashi, N.; Otake, Y.; Yamamura, Y.; Saito, K.; Oshio, H. *J. Am. Chem. Soc.* **2010**, *132*, 3553–3560. (b) Jeannin, O.; Clérac, R.; Fourmigué, M. *Chem. Mater.* **2007**, *19*, 5946–5954. (c) Jeannin, O.; Clérac, R.; Fourmigué, M. *J. Am. Chem. Soc.* **2006**, *128*, 14649–14656. (d) Fourmigué, M. *Acc. Chem. Res.* **2004**, *37*, 179–186. (e) Umezono, Y.; Fujita, W.; Awaga, K. *J. Am. Chem. Soc.* **2006**, *128*, 1084–1085. (f) Willett, R. D.; Gómez-Garcí, C. J.; Ramakrishna, B. L.; Twamley, B. *Polyhedron* **2005**, *24*, 2232–2237.

(7) (a) Kato, R. *Chem. Rev.* **2004**, *104*, 5319–5346. (b) Tanaka, H.; Tokumoto, M.; Ishibashi, S.; Graf, D.; Choi, E. S.; Brooks, J. S.; Yasuzuka, S.; Okano, Y.; Kobayashi, H.; Kobayashi, A. *J. Am. Chem. Soc.* **2004**, *126*, 10518–10519. (c) Zhou, B.; Shimamura, M.; Fujiwara, E.; Kobayashi, A.; Higashi, T.; Nishibori, E.; Sakata, M.; Cui, H. B.; Takahashi, K.; Kobayashi, H. *J. Am. Chem. Soc.* **2006**, *128*, 3872–3873. (d) Nakamura, T.; Akutagawa, T.; Honda, K.; Underhill, A. E.; Coomber, A. T.; Friend, R. H. *Nature* **1998**, *394*, 159–162.

(8) Duan, H. B.; Ren, X. M.; Meng, Q. J. *Coord. Chem. Rev.* **2010**, *254*, 1509–1522.

(9) (a) Duan, H. B.; Zhou, H.; Tian, Z. F.; Xuan, F.; Ren, X. M. *Solid State Sci.* **2009**, *11*, 1216–1221. (b) Umezono, Y.; Wataru Fujita, W.; Awaga, K. *Chem. Phys. Lett.* **2005**, *409*, 139–143. (c) Nakajima, H.; Katsuhara, M.; Ashizawa, M.; Kawamoto, T.; Mori, T. *Inorg. Chem.* **2004**, *43*, 6075–6082.

(10) (a) Ren, X. M.; Meng, Q. J.; Song, Y.; Lu, C. S.; Hu, C. J.; Chen, X. Y. *Inorg. Chem.* **2002**, *41*, 5686–5692. (b) Xie, J. L.; Ren, X. M.; Song, Y.; Zhang, W. W.; Liu, W. L.; He, C.; Meng, Q. J. *Chem. Commun.* **2002**, 2346–2347. (c) Xie, J. L.; Ren, X. M.; He, C.; Song, Y.; Meng, Q. J.; Kremer, R. K.; Yao, Y. G. *Chem. Phys. Lett.* **2003**, *369*, 41–48. (d) Dang, D. B.; Ni, C. L.; Bai, Y.; Tian, Z. F.; Ni, Z. P.; Wen, L. L.; Meng, Q. J.; Gao, S. *Chem. Lett.* **2005**, *34*, 680–681. (e) Ren, X. M.; Akutagawa, T.; Nishihara, S.; Nakamura, T.; Fujita, W.; Awaga, K. *J. Phys. Chem. B* **2005**, *109*, 16610–16615. (f) Tian, Z. F.; Duan, H. B.; Ren, X. M.; Lu, C. S.; Li, Y. Z.; Song, Y.; Zhu, H. Z.; Meng, Q. J. *J. Phys. Chem. B* **2009**, *113*, 8278–8283.

(11) (a) Ren, X. M.; Okudera, H.; Kremer, R. K.; Song, Y.; He, C.; Meng, Q. J.; Wu, P. H. *Inorg. Chem.* **2004**, *43*, 2569–2576. (b) Ren, X. M.; Akutagawa, T.; Nishihara, S.; Nakamura, T. *Synth. Met.* **2005**, *150*, 57–61. (c) Ren, X. M.; Okudera, H.; Xie, J. L.; Meng, Q. J. *J. Mol. Struct.* **2005**, *733*, 119–124. (d) Ren, X. M.; Nishihara, S.; Akutagawa, T.; Noro, S.; Nakamura, T.; Fujita, W.; Awaga., K. *Chem. Phys. Lett.* **2006**, *418*, 423–427.

(12) (a) Xie., J. L.; Ren, X. M.; Tong, W. J.; Song, Y.; Lu, C. S.; Yao, Y. G.; Meng, Q. J. *Inorg. Chem. Commun.* **2002**, *5*, 395–398. (b) Xie, J. L.; Ren, X. M.; Gao, S.; Zhang, W. W.; Li, Y. Z.; Lu, C. S.; Ni, C. L.; Liu, W. L.; Meng, Q. J.; Yao, Y. G. *Eur. J. Inorg. Chem.* **2003**, 2393–2396. (c) Ni, C. L.; Dang, D. B.; Li, Y. Z.; Gao, S.; Ni, Z. P.; Tian, Z. F.; Meng, Q. J. *J. Solid State Chem.* **2005**, *178*, 100–105. (d) Ni, C. L.; Dang, D. B.; Li, Y. Z.; Yuan, Z. R.; Ni, Z. P.; Tian, Z. F.; Meng, Q. J. *Inorg. Chem. Commun.* **2004**, *7*, 1034–1036. (e) Ni, C. L.; Song, Y.; Meng, Q. J. *Chem. Phys. Lett.* **2006**, *419*, 351–355. (f) Ni, C. L.; Li, Y. Z.; Dang, D. B.; Gao, S.; Ni, Z. P.; Tian, Z. F.; Wen, L. L.; Meng, Q. J. *Polyhedron* **2005**, *24*, 1669–1676. (g) Ni, C. L.; Li, Y. Z.; Dang, D. B.; Ni, Z. P.; Tian, Z. F.; Yuan, Z. R.; Meng, Q. J. *Inorg. Chem. Commun.* **2005**, *8*, 105–108.

(13) Davison, A.; Holm, H. R. *Inorg. Synth.* **1967**, *10*, 8–26.

(14) Ren, X. M.; Meng, Q. J.; Song, Y.; Hu, C. J.; Lu, C. S.; Chen, X. Y.; Xue, Z. L. *Inorg. Chem.* **2002**, *41*, 5931–5932.

(15) *SMART and SAINT*; Siemens Analytical X-ray Instrument Inc.: Madison, WI, 1996.

(16) Sheldrick, G. M. *SHELXL-97*, Program for the Refinement of Crystal Structure; University of Göttingen: Göttingen, Germany, 1997.

(17) Frisch, M. J.; Trucks, G. W.; Schlegel, H. B. et al. *Gaussian 98*, Revision A.11; Gaussian, Inc.: Pittsburgh, PA, 2001.

(18) (a) Becke, A. D. *J. Chem. Phys.* **1993**, *98*, 5648–5652. (b) Lee, C.; Yang, W.; Parr, R. G. *Phys. Rev. B* **1988**, *37*, 785–789. (c) Miehlich, B.; Savin, A.; Stoll, H.; Preuss, H. *Chem. Phys. Lett.* **1989**, *157*, 200–206.

(19) Bondi, A. *J. Phys. Chem.* **1964**, *68*, 441–451.

(20) Ren, X. M.; Akutagawa, T.; Noro, S.; Nishihara, S.; Nakamura, T.; Yoshita, Y.; Inoue, K. *J. Phys. Chem. B* **2006**, *110*, 7671–7677.

(21) (a) Carlin, R. L. *Magnetochemistry*; Springer-Verlag: Berlin, Heideberg, 1986; p 202; (b) Stryjewski, E.; Giordano, N. *Adv. Phys.* **1977**, *26*, 487–650.

(22) Baker, G. A.; Rushbrooke, G. S. *Phys. Rev.* **1964**, *135*, 1272–1277.

(23) (a) Lloret, F.; Ruiz, R.; Julve, M.; Faus, J.; Journaux, Y.; Castro, I.; Verdaguer, M. *Chem. Mater.* **1992**, *4*, 1150–1153. (b) Caneschi, A.; Gatteschi, D.; Melandri, M. C.; Rey, P.; Sessoli, R. *Inorg. Chem.* **1990**, *29*, 4228–4234. (c) Thompson, L. K.; Tandon, S. S.; Lloret, F.; Cano, J.; Julve, M. *Inorg. Chem.* **1997**, *36*, 3301–3306.

(24) (a) Ni, Z. P.; Ren, X. M.; Ma, J.; Xie, J. L.; Ni, C. L.; Chen, Z. D.; Meng, Q. J. *J. Am. Chem. Soc.* **2005**, *127*, 14330–14338. (b) Alvarez, S.; Vicente, R.; Hoffmann, R. *J. Am. Chem. Soc.* **1985**, *107*, 6253–6277.